An estimation of the effective number of electrons contributing to the coordinate measurement with a TPC II

Makoto Kobayashi

High Energy Accelerator Research Organization (KEK), Tsukuba, 305-0801, Japan

Abstract

For time projection chambers the accuracy in measurement of track coordinates along the pad-row direction deteriorates with the drift distance (z): $\sigma_{\rm X}^2 \sim D^2 \cdot z/N_{\rm eff}$, where D is the diffusion constant and $N_{\rm eff}$ is the effective number of electrons. Experimentally it has been shown that $N_{\rm eff}$ is smaller than the average number of drift electrons per pad row ($\langle N \rangle$). In the previous work we estimated $N_{\rm eff}$ by means of a simple numerical simulation, taking into account the diffusion of electrons only in the pad-row direction [1]. The simulation showed that $N_{\rm eff}$ could be as small as $\sim 30\%$ of $\langle N \rangle$ because of the combined effect of statistical fluctuations in the number of drift electrons (N) and in their multiplication in avalanches. In this paper, we evaluate the influence of the diffusion along the direction of pad-row normal on the effective number of electrons.

Keywords:
TPC, Resolution, Effective Number of Electrons, Diffusion, Simulation, MPGD
PACS: 29.40.Cs, 29.40.Gx

1. Introduction

In the previous paper we estimated the effective number of electrons ($N_{\rm eff}$) contributing to the coordinate measurement of a time projection chamber (TPC) equipped with a Micro-Pattern GAS Detector (MPGD) and ideal readout electronics [1]. $N_{\rm eff}$ parametrizes the spatial resolution for a pad row as follows

$$\sigma_{\rm X}^2 = \sigma_{\rm X0}^2 + \frac{D^2}{N_{\rm eff}} \cdot z \tag{1}$$

where $\sigma_{\rm X}$ is the spatial resolution along the pad-row direction, $\sigma_{\rm X0}$ is the intrinsic resolution, and D denotes the transverse diffusion constant, with z being the drift distance. In the ideal case (with an infinitesimal pad pitch) $\sigma_{\rm X0}$ vanishes for particle tracks perpendicular to the pad row, and increases with the track angle (ϕ) with respect to the pad-row normal because of the angular pad effect. Only right angle tracks ($\phi = 0^\circ$) are considered throughout the present work.

Under the conditions listed in Ref. [1], $N_{\rm eff}$ is given by

$$\frac{1}{N_{\rm eff}} = \left\langle \frac{1}{N} \right\rangle \cdot (1 + f) \tag{2}$$

where N denotes the total number of drift electrons detected by the pad row and $f = \sigma_q^2 / \langle q \rangle^2$, with q being the signal charge induced on the pad row by single drift electrons[1]. Although Eq. (2)

[1] It should be noted that Eq. (2) is an expression for $1/N(h)$ in Eq. (7.33) of Ref. [2].

was derived assuming the total charge ($\sum_{i=1}^{N} q_i$) to be constant ($N \cdot \langle q \rangle$) it was found to be a good approximation by a numerical simulation for a practical value of $\langle N \rangle$ (see Ref. [1], and Appendix A for details).

The simulation for argon-based gas mixtures gave $N_{\rm eff}$ of ~ 22 for $f = 2/3$ and a pad-row pitch of 6.3 mm [1], which is about 30% of the average value of N ($\langle N \rangle \sim 71$), and is consistent with the values obtained with a small prototype TPC [3–5]. The value of $N_{\rm eff}$ corresponds to ~ 36 for a pad-row pitch normalized to 1 cm, assuming $N_{\rm eff}$ to be (approximately) proportional to the pad-row pitch[2].

Recent resolution measurements with a larger prototype TPC with MicroMEGAS readout, however, gave a significantly larger estimate for $N_{\rm eff}$ (~ 56 for 1-cm pad height) [6][3]. A possible origin of the discrepancy could be the de-clustering of drift electrons due to diffusion along the direction of the pad-row normal ($D_{\rm y}$), which is expected to be more efficient for larger TPCs with a longer average drift distance. It should be pointed out that the diffusion only along the pad-row direction ($D_{\rm x}$) was taken into account in Ref. [1]. In the present work, we evaluate the contribution of the de-clustering effect to the increase of $N_{\rm eff}$, through the decrease of $\langle 1/N \rangle$ due to the finite $D_{\rm y}$.

A hypothetical case of an infinitely large TPC is considered in Section 2, a more practical case is qualitatively discussed in Section 3, the results of a realistic simulation are shown in Section 4, and Section 5 concludes the paper. Readers are suggested to have read Ref. [1] in advance.

2. In the case of infinitely large TPC

Let us consider the hypothetical case of a TPC with infinitely large drift distance and readout plane. Primary ionization clusters created along a particle track at infinitely large drift distance get completely de-clustered and the total number of drift electrons reaching a pad row obeys Poisson statistics with a mean $\mu = \langle N \rangle$:

$$P(N) = e^{-\mu} \cdot \frac{\mu^N}{N!} \ .$$

The dimensions of the readout pad plane are considered to be large enough. Otherwise a part of the drift electrons created at long drift distances would be absorbed by the field cage (the inner or outer wall of cylindrical TPC) before reaching the readout plane.

The average value of the inverse of N in this case is given by

$$\begin{aligned} \left\langle \frac{1}{N} \right\rangle &= \sum_{N=1}^{\infty} \frac{1}{N} \cdot P(N) \\ &= e^{-\mu} \cdot \sum_{N=1}^{\infty} \frac{\mu^N}{N \cdot N!} \\ &= (E_i(\mu) - \ln(\mu) - \gamma) \cdot e^{-\mu} \end{aligned}$$

where E_i is the exponential integral[4] and γ is the Euler-Mascheroni constant (~ 0.577). When $N = 0$ the pad row is inefficient and provides no coordinate measurement. Therefore it is excluded from

[2] Actually, this is a bold assumption. See Appendix A.

[3] In fact, the values of $N_{\rm eff}$ were obtained using different kinds of charged particle: a beam of 5-GeV/c electrons in Ref. [6] while a beam of 4-GeV/c pions or cosmic rays in Refs. [3–5]. The discrepancy is still large, however, even if the difference in the primary ionization density is taken into account.

[4] The exponential integral is defined as

$$E_i(x) = \int_{-\infty}^{x} \frac{e^t}{t} \, dt \ .$$

the summation. Fig. 1 shows the behavior of $R_{\rm N} \equiv \langle N \rangle \cdot \langle 1/N \rangle$ as a function of $\langle N \rangle$. For a practical value of $\langle N \rangle \gtrsim 50$, $\langle 1/N \rangle \sim 1/\langle N \rangle$ and $N_{\rm eff}$ is expected to be $\sim \langle N \rangle /(1+f)$.

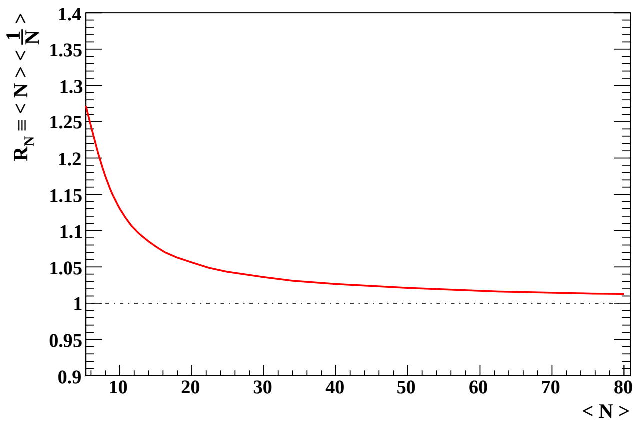

Figure 1: $R_{\rm N} \equiv \langle N \rangle \cdot \langle 1/N \rangle$ as a function of the average number of electrons in the case of Poisson distribution for N.

For a finite drift distance $N_{\rm eff} < \langle N \rangle /(1+f)$ because of broad and asymmetric distribution of N (Landau tail) even for relatively large $\langle N \rangle$. For long drift distances the distribution approaches a Poissonian, which is close to a Gaussian for $\langle N \rangle \gtrsim 20$. Consequently, $N_{\rm eff}$ is expected to be an increasing function of the drift distance (z) with an asymptotic maximum of $\sim \langle N \rangle /(1+f)$.

3. In the case of real TPC

We evaluate in this section the variance (Var) of the total number of electrons reaching a readout pad row (N) since Var(N) gives a good measure for the deviation of N-distribution from a Poissonian, for which Var(N) $= N$. First, let us suppose that a single point-like electron cluster of size n is created at a coordinate $y = Y$ in the direction of the pad-row normal and $z = Z$ in the drift direction, measured from the readout plane. The electrons diffuse on their way towards the readout plane. Their spread in the y-coordinate is given by a Gaussian with a standard deviation of $\sigma \equiv \sigma_y = D \cdot \sqrt{Z}$, at the pad rows with a height of h[5]. The probability to find ν electrons reaching the pad row is given by[6]

$$P(\nu; Y, \sigma) = \binom{n}{\nu} \cdot \Pi^{\nu}(Y) \cdot (1 - \Pi(Y))^{n-\nu}$$

where

$$\Pi(Y) = \int_{-h/2}^{h/2} G(y; Y, \sigma)\, dy$$

with

$$G(y; Y, \sigma) \equiv \frac{1}{\sqrt{2\pi}\sigma} \cdot \exp\left[-\frac{(y-Y)^2}{2\sigma^2} \right] .$$

[5] More precisely h should be understood as the pad-row pitch, which is usually slightly larger than the pad height when the readout plane is covered over with pads. The pad-row pitch and the pad height (h) are not distinguished in the present paper.

[6] Hereafter the notation $f^n(x)$ represents the n-th power of a function $f(x)$, i.e. $(f(x))^n$.

Since $P(\nu; Y, \sigma)$ represents a binomial statistics for a fixed Y (and σ), $\langle\nu\rangle$ and $\langle\nu^2\rangle$ are given by

$$\langle\nu(Y)\rangle = n \cdot \Pi(Y)$$

and

$$\left\langle\nu^2(Y)\right\rangle = n \cdot \Pi(Y) + n(n-1) \cdot \Pi^2(Y) \ .$$

Let us further assume that the initial cluster is randomly created in a y-region $[-H/2, +H/2]$ with $H \gg \sigma$ (see Fig. 2). Then, averaging over $-H/2 \le Y \le +H/2$,

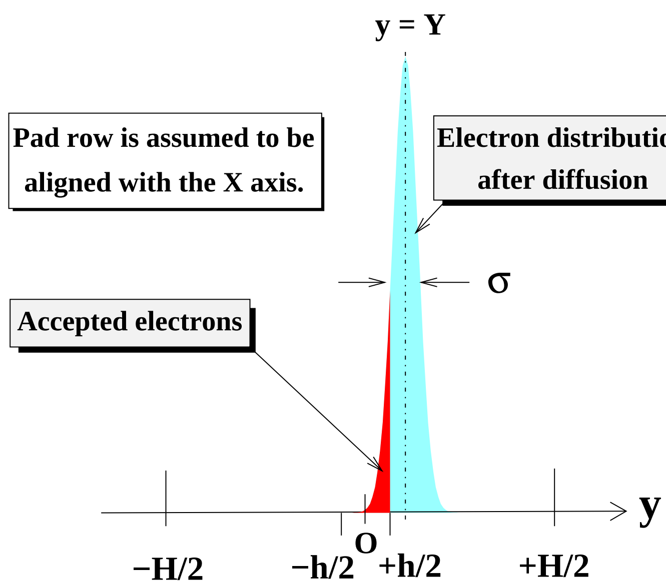

Figure 2: Illustration of the relevant variables.

$$\begin{aligned}
\langle\nu\rangle &= \frac{1}{H}\int_{-H/2}^{H/2} \langle\nu(Y)\rangle \, dY \\
&= \frac{n}{H}\int_{-H/2}^{H/2} dY \int_{-h/2}^{h/2} G(y; Y, \sigma)\, dy \\
&= \frac{n}{H}\int_{-h/2}^{h/2} dy \int_{-H/2}^{H/2} G(y; Y, \sigma)\, dY \\
&\sim \frac{n \cdot h}{H} \\
\mathrm{Var}(\nu) &= \frac{1}{H}\int_{-H/2}^{H/2} \left\langle\nu^2(Y)\right\rangle \, dy - \langle\nu\rangle^2 \\
&\sim \frac{n \cdot h}{H} + \frac{n(n-1)}{H}\int_{-H/2}^{H/2} \Pi^2(Y)\, dY - \left(\frac{n \cdot h}{H}\right)^2 \\
&\sim \frac{n \cdot h}{H} + \frac{n(n-1)}{H} \cdot h \cdot g\left(\frac{\sigma}{h}\right) - \left(\frac{n \cdot h}{H}\right)^2
\end{aligned}$$

where

$$g\left(\frac{\sigma}{h}\right) \equiv \operatorname{erf}\left(\frac{h}{2\sigma}\right) - \frac{2}{\sqrt{\pi}} \cdot \frac{\sigma}{h} \cdot \left[1 - \exp\left(-\frac{h^2}{4\sigma^2}\right)\right] .$$

See Appendix B for the derivation of function $g(\sigma/h)$.

If there are $N_{\rm CL}$ (independent) clusters in $[-H/2, +H/2]$, the average and the variance are given by multiplying $N_{\rm CL}$[7]:

$$\begin{aligned} \langle \nu \rangle &= \frac{N_{\rm CL}}{H} \cdot n \cdot h \\ \operatorname{Var}(\nu) &= \frac{N_{\rm CL}}{H} \cdot n \cdot h + \frac{N_{\rm CL}}{H} \cdot n(n-1) \cdot h \cdot g\left(\frac{\sigma}{h}\right) - N_{\rm CL} \cdot \left(\frac{n \cdot h}{H}\right)^2 . \end{aligned}$$

Taking the limit of $H \to \infty$ while keeping the cluster density $\rho \equiv N_{\rm CL}/H$ constant,

$$\begin{aligned} \langle \nu \rangle &= \rho \cdot n \cdot h \\ \operatorname{Var}(\nu) &= \rho \cdot n \cdot h + \rho \cdot n(n-1) \cdot h \cdot g\left(\frac{\sigma}{h}\right) . \end{aligned}$$

In reality the cluster density (ρ) depends on the cluster size (n):

$$\rho = \rho(n) \equiv \rho_0 \cdot p(n)$$

where ρ_0 is the total primary ionization density and $p(n)$ is the proportion of the cluster of size n ($\sum_n p(n) = 1$). The number of electrons detected by the pad row (N) is the sum of the contribution (ν) from various cluster sizes. Consequently, its average and variance are given by

$$\begin{aligned} \langle N \rangle &= \rho_0 \cdot h \cdot \sum_n n \cdot p(n) \\ \operatorname{Var}(N) &= \rho_0 \cdot h \cdot \sum_n n \cdot p(n) \cdot \left(1 + (n-1) \cdot g\left(\frac{\sigma}{h}\right)\right) . \end{aligned}$$

Fig. 3 (a) shows

$$\frac{\operatorname{Var}(\nu)}{\langle \nu \rangle} = 1 + (n-1) \cdot g\left(\frac{\sigma}{h}\right)$$

for several values of the cluster size n as a function of the scaling parameter σ/h. It is clear that ν distribution approaches a Poissonian ($\operatorname{Var}(\nu)/\langle \nu \rangle = 1$) slowly with the increase of σ/h, especially for large clusters. Fig. 3 (b) shows the variance divided by the average for a realistic N-distribution:

$$\begin{aligned} \frac{\operatorname{Var}(N)}{\langle N \rangle} &= \frac{\sum_n n \cdot p(n) \cdot \left(1 + (n-1) \cdot g\left(\frac{\sigma}{h}\right)\right)}{\sum_n n \cdot p(n)} \\ &= 1 + \frac{\sum_n n(n-1) \cdot p(n)}{\sum_n n \cdot p(n)} \cdot g\left(\frac{\sigma}{h}\right) , \end{aligned}$$

along with the ratios obtained with a numerical simulation (see below). The probability mass function $p(n)$ was assumed to be that corresponding to the cluster-size distribution shown in Fig. 2 of Ref. [1].

---

[7] Note that

$$\left\langle \sum_{i=1}^{N_{\rm CL}} \nu_i \right\rangle = N_{\rm CL} \cdot \langle \nu \rangle \quad \text{and}$$

$$\left\langle \left(\sum_{i=1}^{N_{\rm CL}} \nu_i - \left\langle \sum_{i=1}^{N_{\rm CL}} \nu_i \right\rangle \right)^2 \right\rangle = \left\langle \left(\sum_{i=1}^{N_{\rm CL}} (\nu_i - \langle \nu_i \rangle) \right)^2 \right\rangle = N_{\rm CL} \cdot \left\langle (\nu - \langle \nu \rangle)^2 \right\rangle .$$

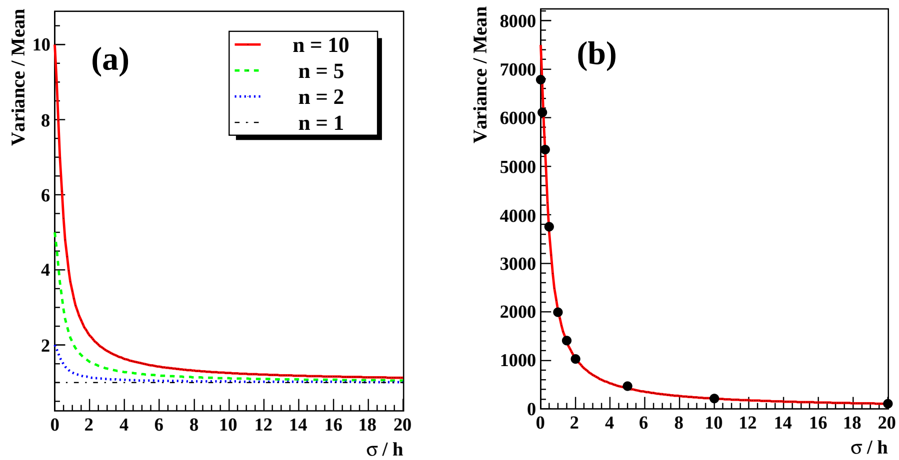

Figure 3: Variance divided by mean as a function of the scaling parameter σ/h: (a) for several fixed values of the cluster size and (b) for a realistic cluster-size distribution along with the *data points* given by a numerical simulation (filled circles).

4. Evaluation of $N_{\rm eff}$ by simulation

The analytic approach described in Section3 shows that $N_{\rm eff}$ is expected to be a slowly increasing function of σ/h, i.e. the drift distance. In order to confirm this quantitatively, we evaluated $N_{\rm eff}$ by means of a numerical simulation.

The simulation code is identical to that used in the previous work [1], except that the diffusion of drift electrons in the the direction of pad-row normal ($D_{\rm y}$) is taken into account. Initial electron clusters are randomly generated along the y-axis (with the pad row aligned with the x-axis) in a range wide enough compared to the diffusion ($\sigma = D \cdot \sqrt{Z}$) and the pad height ($h$). The cluster density is assumed to be 24.3 cm^{-1} $\times$ 1.2 (relativistic rise factor) as in the previous paper [1]. The size of each cluster is determined randomly using the probability mass function $p(n)$ (see Section 3). The secondary electrons originated from each cluster are then dispersed in the directions of pad row (x) and pad-row normal (y) with $\sigma_x = \sigma_y = \sigma = D \cdot \sqrt{Z}$ [8]. The electrons with the final position located within the pad row ($|y| < h/2$) are accepted (see Fig 2). Gas gain is assigned to each accepted electron randomly assuming a Polya distribution ($\theta = 0.5$, corresponding to $f = 2/3$) for the avalanche fluctuation. The coordinate resolution ($\sigma_{\rm X}$) is calculated using the charge centroid of the accepted electrons in the pad-row direction (x). The square of the ratio of the diffusion (σ) to the resolution ($\sigma_{\rm X}$) gives $N_{\rm eff}$ from Eq. (1) with $\sigma_{\rm X0} = 0$.

Fig. 4 shows the obtained $N_{\rm eff}$ and $\langle 1/N \rangle^{-1}$ as a function of σ/h. The effective number of electrons certainly increases with σ/h in association with the increase of $\langle 1/N \rangle^{-1}$. However, the increase of $N_{\rm eff}$ is rather slow and would be observable only for large values of σ/h, i.e. at (very) long drift distances. Examples of the resolution squared as a function of the drift distance are shown in Fig. 5 for pad heights of 6.3 mm and 3.15 mm. The chamber gas is taken to be Ar-CF4 (3%)-isobutane (2%) as in the experiments of Refs. [5, 6]. The deviation from the linear dependence (Eq. (1) with a constant $N_{\rm eff}$) is prominent at long drift distances without magnetic field, in particular for a shorter pad height.

[8] Note that $D_x = D_y = D$ since the magnetic field (if it exists) is parallel to the z-axis.

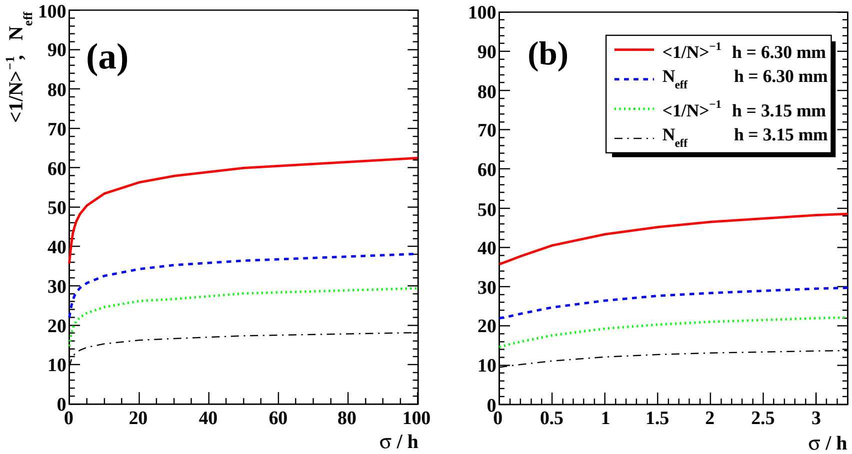

Figure 4: Inverse of the average of $1/N$ and effective number of electrons as a function of σ/h for $h = 6.30$ mm and 3.15 mm. The values for small (realistic) σ/h are shown in (b).

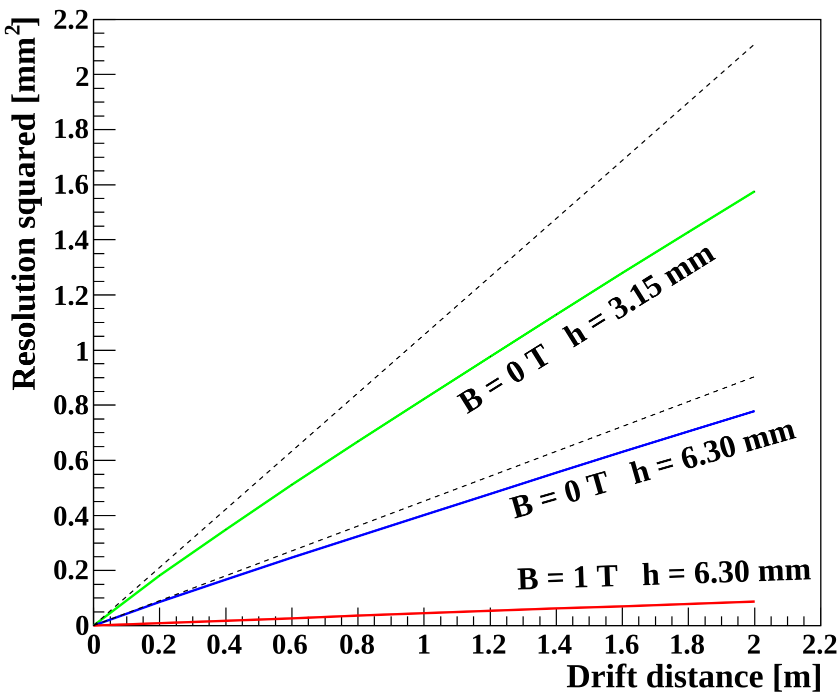

Figure 5: Resolution squared as a function of the drift distance (z) given by the simulation for $B = 0$ and 1 T, with a pad height (h) of 6.3 mm. The diffusion constant is assumed to be 315 (101) μm/$\sqrt{\text{cm}}$ for B= 0 (1) T given by Magboltz [7] for a gas mixture of Ar-CF4 (3%)-isobutane (2%) and a drift field of 250 V/cm. The relation simulated for $B = 0$ T with $h = 3.15$ mm is also shown for comparison. The dashed straight lines show the linear relations with the values of N_{eff} fixed to those at $z = 0$, in the case of $B = 0$ T. For $B = 1$ T, N_{eff} is almost constant throughout the drift distance shown in the figure.

5. Conclusion

We estimated the effect of the electron diffusion along the direction of pad-row normal ($D_{\rm y}$) on the spatial resolution of TPCs operated in argon-based gases. It does affect the effective number of electrons contributing to the azimuthal coordinate measurement. The value of $N_{\rm eff}$ increases with the drift distance since the distribution of the number of electrons detected by a pad row approaches a Poissonian by de-clustering. However, the de-clustering process is rather slow because its scaling parameter is σ/h, and $N_{\rm eff}$ can be assumed to be constant for practical TPCs.

Furthermore, the effect of avalanche fluctuation ($R_{\rm q}$) was found to be almost constant ($\sim 1+f$) for a realistic pad-row pitch greater than $\sim$ 6 mm (see Appendix A). Therefore Eq. (2) is expected to be an appropriate expression for the value of $N_{\rm eff}$, with $\langle 1/N \rangle$ estimated with $D_{\rm y} = 0$.

It is unlikely that the increase of $N_{\rm eff}$ observed with a large TPC prototype, with the maximum drift length of $\sim$ 600 mm, arises from the finite $D_{\rm y}$. The larger $N_{\rm eff}$ may have been owing to other factors such as smaller avalanche fluctuations (f), or improvement of the signal-to-noise ratio and/or better calibration of the readout electronics (see Appendix C of Ref. [5]).

The increase of $N_{\rm eff}$ would be observed at long drift distances with a large TPC operated in a gas with a relatively large transverse diffusion constant in the absence of magnetic field.

Acknowledgments

We would like to thank many colleagues of the LCTPC collaboration for their continuous encouragement and support, and for fruitful discussions. This work was partly supported by the Specially Promoted Research Grant No. 23000002 of Japan Society for the Promotion of Science.

Appendix A. Pad-height dependence of $N_{\rm eff}$

In the previous work, the pad-row pitch ($\sim$ pad height h) was fixed to 6.3 mm [1]. We show here the pad-height dependence of the effective number of electrons given by a numerical simulation. The simulation code is exactly the same as that developed for Ref. [1]. Therefore the diffusion of drift electrons in the direction of pad-row normal ($D_{\rm y}$) is not taken into account and the values of $N_{\rm eff}$ are those for zero drift distance.

If we write $N_{\rm eff} = \langle N \rangle / R$, with R being a reduction factor, R is expressed as $R = R_{\rm N} \cdot R_{\rm q}$, where $R_{\rm N} = \langle N \rangle \cdot \langle N^{-1} \rangle$ and $R_{\rm q}$ derives from the avalanche fluctuation in the detection device for each of drift electrons. The value of $R_{\rm q}$ is expected to be close to $1+f$ for large $\langle N \rangle$ (large pad height) since $\sum_{i=1}^{N} q_i \sim N \cdot \langle q \rangle$ becomes a good approximation. Fig. A.1 shows the pad-height dependences of $R_{\rm N}$, $R_{\rm q}$ and R. The relative variance of avalanche fluctuation (f) is assumed to be 2/3. The value of $R_{\rm q}$ is almost constant ($\sim 1+f$) for practical pad heights ($\gtrsim$ 6 mm) whereas $R_{\rm N}$ is a decreasing function of the pad height as expected.

The values of $\langle 1/N \rangle^{-1}$ ($= \langle N \rangle / R_{\rm N}$) and $N_{\rm eff}$ are plotted in Fig. A.2 against the pad height, along with $\langle N \rangle$. It is clear that $N_{\rm eff}$ is not a linear function of the pad height because of $R_{\rm N}$ decreasing with the pad height. The effective number of electrons is about 31% (43%) of $\langle N \rangle$ for a pad height of 6.3 mm (100.8 mm).

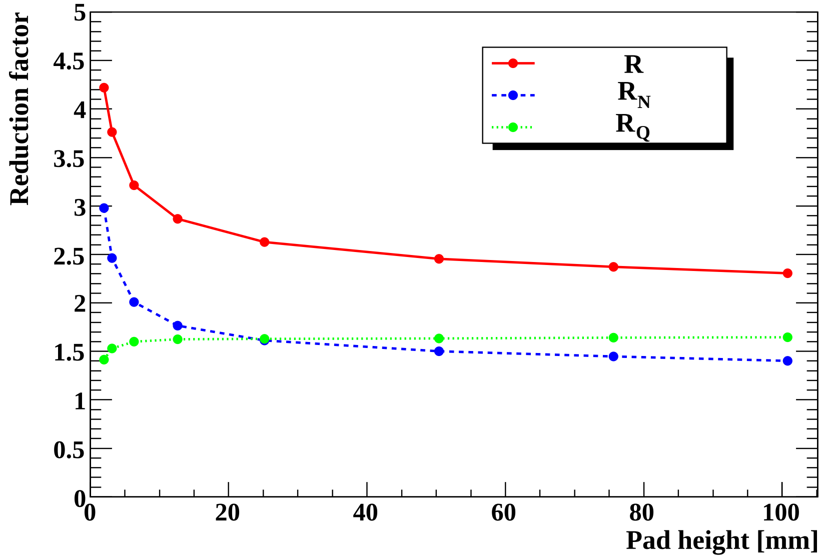

Figure A.1: Reduction factors (R, R_N and R_q) as a function of the pad height.

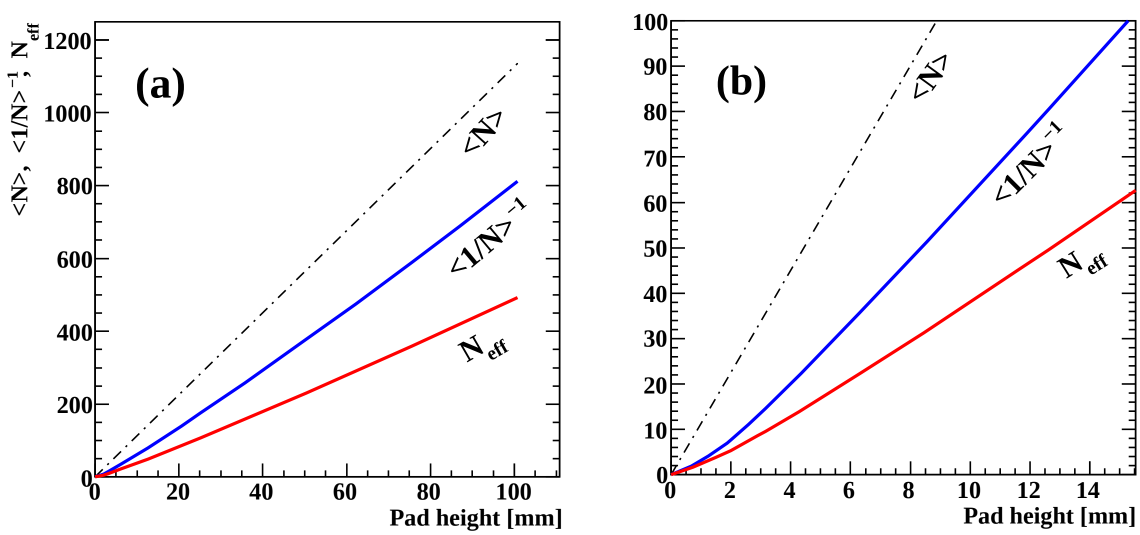

Figure A.2: (a) Average number of electrons ($\langle N\rangle$), inverse of the average of $1/N$ ($\langle 1/N\rangle^{-1}$), and effective number of electrons ($N_{\rm eff}$) as a function of the pad height. (b) Details for small pad heights.

Appendix B. Derivation of function g

In this appendix we derive the explicit expression of the function $g(\sigma/h)$ used to evaluate $\mathrm{Var}(\nu)$ in Section 3. The function is defined as

$$h \cdot g\left(\frac{\sigma}{h}\right) = \lim_{H\to\infty} \int_{-H/2}^{H/2} \Pi^2(Y)\, dY = \int_{-\infty}^{\infty} \Pi^2(Y)\, dY$$

where

$$\Pi(Y) = \int_{-h/2}^{h/2} G(y; Y, \sigma)\, dy$$

with

$$G(y; Y, \sigma) \equiv \frac{1}{\sqrt{2\pi}\sigma} \cdot \exp\left[-\frac{(y-Y)^2}{2\sigma^2}\right] .$$

Let us carry out the integration on the right hand side of the equation:

$$\begin{aligned}
\int_{-\infty}^{\infty} \Pi^2(Y)\, dY &= \frac{1}{2\pi\sigma^2} \int_{-\infty}^{\infty} \left[\int_{-h/2}^{h/2} \exp\left(-\frac{(y-Y)^2}{2\sigma^2}\right) dy \cdot \int_{-h/2}^{h/2} \exp\left(-\frac{(y\prime-Y)^2}{2\sigma^2}\right) dy\prime\right] dY \\
&= \frac{1}{2\pi\sigma^2} \int_{-\infty}^{\infty} dY \int_{-h/2}^{h/2} dy \int_{-h/2}^{h/2} dy\prime\, \exp\left[-\frac{1}{2\sigma^2}\left((y-Y)^2 + (y\prime-Y)^2\right)\right] \\
&= \frac{1}{2\pi\sigma^2} \int_{-\infty}^{\infty} dY \int_{-h/2}^{h/2} dy \int_{-h/2}^{h/2} dy\prime\, \exp\left[-\frac{1}{\sigma^2}\left(Y - \frac{y+y\prime}{2}\right)^2 - \frac{1}{4\sigma^2}(y-y\prime)^2\right] \\
&= \frac{1}{2\sqrt{\pi}\sigma} \int_{-h/2}^{h/2} dy \int_{-h/2}^{h/2} dy\prime\, \exp\left[-\frac{1}{4\sigma^2}(y-y\prime)^2\right] \\
&= \frac{2}{\sqrt{\pi}\sigma} \int_0^{h/\sqrt{2}} d\xi \int_0^{h/\sqrt{2}-\xi} \exp\left(-\frac{\eta^2}{2\sigma^2}\right) d\eta \\
&\qquad\qquad \text{with } \xi = \frac{(y\prime+y)}{\sqrt{2}} \text{ and } \eta = \frac{(y\prime-y)}{\sqrt{2}} \\
&= \frac{2h}{\sqrt{\pi}} \int_0^1 du \int_0^{h\cdot(1-u)/2\sigma} \exp(-v^2)\, dv \\
&\qquad\qquad \text{with } u = \frac{\sqrt{2}}{h}\xi \text{ and } v = \frac{\eta}{\sqrt{2}\sigma} \\
&= h \int_0^1 f(u)\, du \\
&\qquad\qquad \text{with } f(u) = \frac{2}{\sqrt{\pi}} \int_0^{h\cdot(1-u)/2\sigma} \exp(-v^2)\, dv \\
&= h \cdot \left([uf(u)]_0^1 - \int_0^1 uf\prime(u)\, du\right) \\
&= \frac{h^2}{\sqrt{\pi}\sigma} \int_0^1 u \cdot \exp\left[-\left(\frac{h\cdot(1-u)}{2\sigma}\right)^2\right] du \\
&= \frac{2h}{\sqrt{\pi}} \int_0^{h/2\sigma} \left(1 - \frac{2\sigma}{h}t\right) \cdot \exp(-t^2)\, dt \\
&\qquad\qquad \text{with } t = \frac{h\cdot(1-u)}{2\sigma} \\
&= h \cdot \left(\mathrm{erf}\left(\frac{h}{2\sigma}\right) - \frac{4\sigma}{\sqrt{\pi}h} \int_0^{h/2\sigma} t \cdot \exp(-t^2)\, dt\right)
\end{aligned}$$

$$= \quad h \cdot \left(\mathrm{erf}\left(\frac{h}{2\sigma}\right) - \frac{2\sigma}{\sqrt{\pi} h} \int_0^{h^2/4\sigma^2} \exp(-w)\, dw \right)$$

with $w = t^2$

$$= \quad h \cdot \left[\mathrm{erf}\left(\frac{h}{2\sigma}\right) + \frac{2\sigma}{\sqrt{\pi} h} \cdot \left(\exp\left(-\frac{h^2}{4\sigma^2}\right) - 1 \right) \right] .$$

Hence,

$$g\left(\frac{\sigma}{h}\right) = \mathrm{erf}\left(\frac{h}{2\sigma}\right) - \frac{1}{\sqrt{\pi}} \cdot \frac{2\sigma}{h} \cdot \left[1 - \exp\left(-\frac{h^2}{4\sigma^2}\right) \right] .$$

It should be noted that the error function is given by

$$\mathrm{erf}(x) = \frac{2}{\sqrt{\pi}} \int_0^x e^{-t^2}\, dt$$

and that

$$g(0) = \mathrm{erf}(\infty) = 1 \quad \text{and} \quad g(\infty) = 0 .$$

References

[1] M. Kobayashi, Nucl. Instr. and Meth. A 562 (2006) 136.

[2] W. Blum, W. Riegler and L. Rolandi, Particle Detection with Drift Chambers, Springer-Verlag, 2008.

[3] M. Kobayashi, et al., Nucl. Instr. and Meth. A 581 (2007) 265;
M. Kobayashi, et al., Nucl. Instr. and Meth. A 584 (2008) 444.

[4] D.C. Arogancia, et al., Nucl. Instr. and Meth. A 602 (2009) 403.

[5] M. Kobayashi, et al., Nucl. Instr. and Meth. A 641 (2011) 37.

[6] R. Yonamine, JINST 7 (2012) C06011.

[7] S.F. Biagi, Nucl. Instr. and Meth. A 421 (1999) 234.